Hexagonal finite difference operators and 3-d wave equation migration

Marta Woodward and *Francis Muir*

Introduction

The preceding paper demonstrated that regular hexagonal meshes are optimally efficient for sampling circularly bandlimited signals. In this paper it will be shown that hexagonal difference operators corresponding to regular hexagonal sampling meshes are similarly efficient for approximating circularly symmetric operators. Following are comparisons of square and hexagonal difference operator representations of the two-dimensional space domain Laplacian (∇^2)—specifically as they might appear in explicit and implicit 3-d migration schemes. The explicit operators are designed according to Taylor series techniques described below and evaluated in the spatial frequency domain both on their circularity and their match with the ideal operator. Stability considerations are reserved for a later paper. All examples are worked on the square and hexagonal meshes illustrated in Figure 1, related such that their respective bandregions encompass an inscribed, circular region of radius $2\pi/\sqrt{3}h$. To facilitate comparison, the remainder of this paper assumes the Nyquist frequency of interest to be the radius of this inscribed circle.

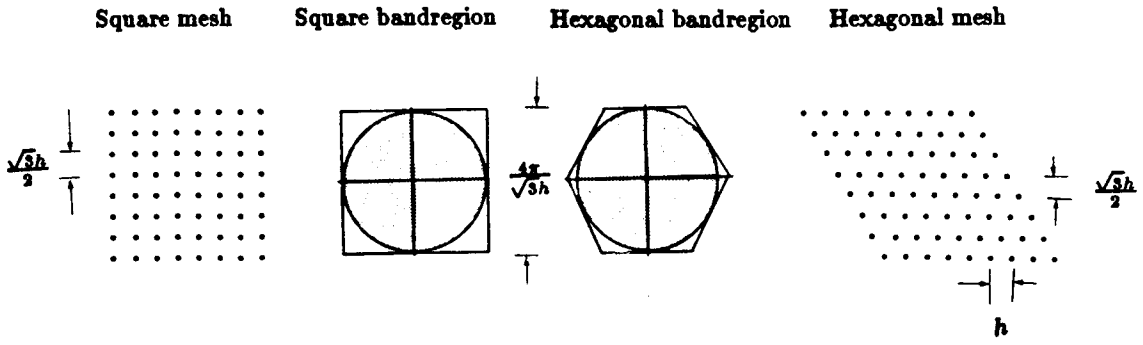

FIG. 1. Square and hexagonal sampling meshes with comparable bandregions.

Explicit schemes: 15 degree wave equation

Ignoring stability, successful explicit 3-d migration with the 15 degree paraxial wave equation

$$\frac{\partial P}{\partial z} \approx \frac{-i\omega}{v} - \frac{v}{-2i\omega}\nabla^2 \tag{1}$$

depends upon the accuracy of the difference formula used in approximating ∇^2. While the two-dimensional Laplacian is usually represented as a sum of one-dimensional second derivatives in two orthogonal directions

$$\nabla^2 = \frac{\partial^2}{\partial x^2} + \frac{\partial^2}{\partial y^2}, \tag{2}$$

it may more generally be represented as a summation of one-dimensional second derivatives in any n symmetrically distributed directions

$$\nabla^2 = \frac{2}{n}\sum_{i=1}^{n} \frac{\partial^2}{\partial x_i^2} \tag{3}$$

($n \geq 2$; see Appendix for proof). This continuous equation may be adapted to a discrete form appropriate for generating difference equations in two steps. First, $\partial^2/\partial x_i^2$ is replaced with the series expansion

$$\frac{\partial^2}{\partial x_i^2} = \frac{\delta^2}{\delta x_i^2} - \frac{\Delta x_i^2}{12}\frac{\delta^4}{\delta x_i^4} + \frac{\Delta x_i^4}{90}\frac{\delta^6}{\delta x_i^6} - \cdots, \tag{4}$$

where $\delta^2/\delta x_i^2$ and $\delta^4/\delta x_i^4$ correspond to the operators $\left(z^{-\Delta x_i} - 2 + z^{\Delta x_i}\right)/\Delta x_i^2$ and $\left(z^{-2\Delta x_i} - 4z^{-\Delta x_i} + 6 - 4z^{\Delta x_i} + z^{2\Delta x_i}\right)/\Delta x_i^4$, respectively (Mitchell, 1980). Second, n—the number of identical, symmetrically distributed directions summed over—is recognized as a fixed, mesh dependent parameter (Figure 2).

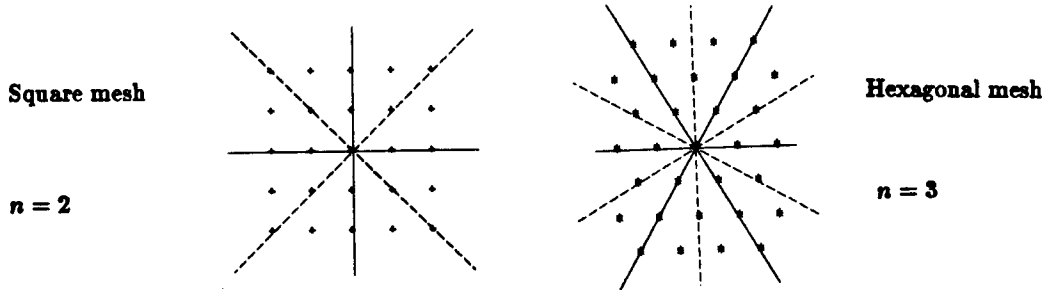

FIG. 2. n symmetrically distributed directions characteristic of square and hexagonal sampling meshes.

The resulting discrete Laplacian is the infinite operator

$$\nabla^2 = \frac{2}{n}\sum_{i=1}^{n}\left(\frac{\delta^2}{\delta x_i{}^2} - \frac{\Delta x_i{}^2}{12}\frac{\delta^4}{\delta x_i{}^4} + \frac{\Delta x_i{}^4}{90}\frac{\delta^6}{\delta x_i{}^6} - \cdots\right), \tag{5}$$

where n and Δx_i are characteristics of the relevant sampling lattice.

A. Leggy operators

Given the difficulty of convolving an infinite operator across sample space, finite, one-dimensional second derivative operators are regularly designed by truncating the Taylor series of equation (4). Application of this method to two dimensions yields the leggy, square and hexagonal difference stars of Figures 4a, 4b and 4c—corresponding to truncations of equation (5) at $\delta^2/\delta x_i{}^2$ (accurate on the order of $\Delta x_i{}^2$), $\delta^4/\delta x_i{}^4$ (accurate on the order of $\Delta x_i{}^4$) and $\delta^6/\delta x_i{}^6$ (accurate on the order of $\Delta x_i{}^6$), respectively. Shown along with the difference stars are plots both of their Fourier transforms and of the relative differences (errors) between their transforms and the true Laplacian of Figure 3.

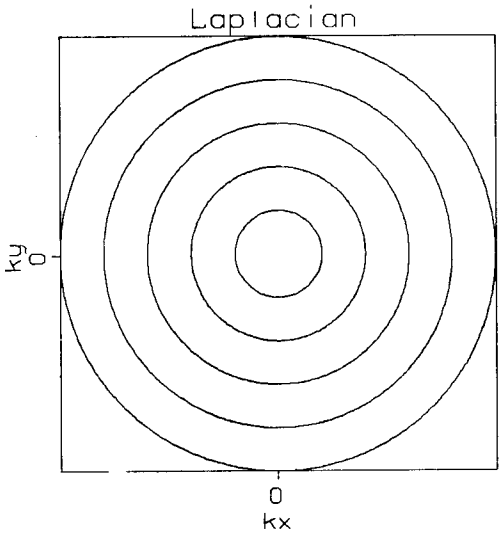

FIG. 3. Frequency domain representation of the true Laplacian: $k_x{}^2 + k_y{}^2$.

Comparison of the figures yields two conclusions: first, as expected from their Taylor series origins, the square and hexagonal operators imitate the true Laplacian comparably well near the origin and comparably poorly near the circular Nyquist; second, the hexagonal operators are consistently more successful at approximating the Laplacian's circular

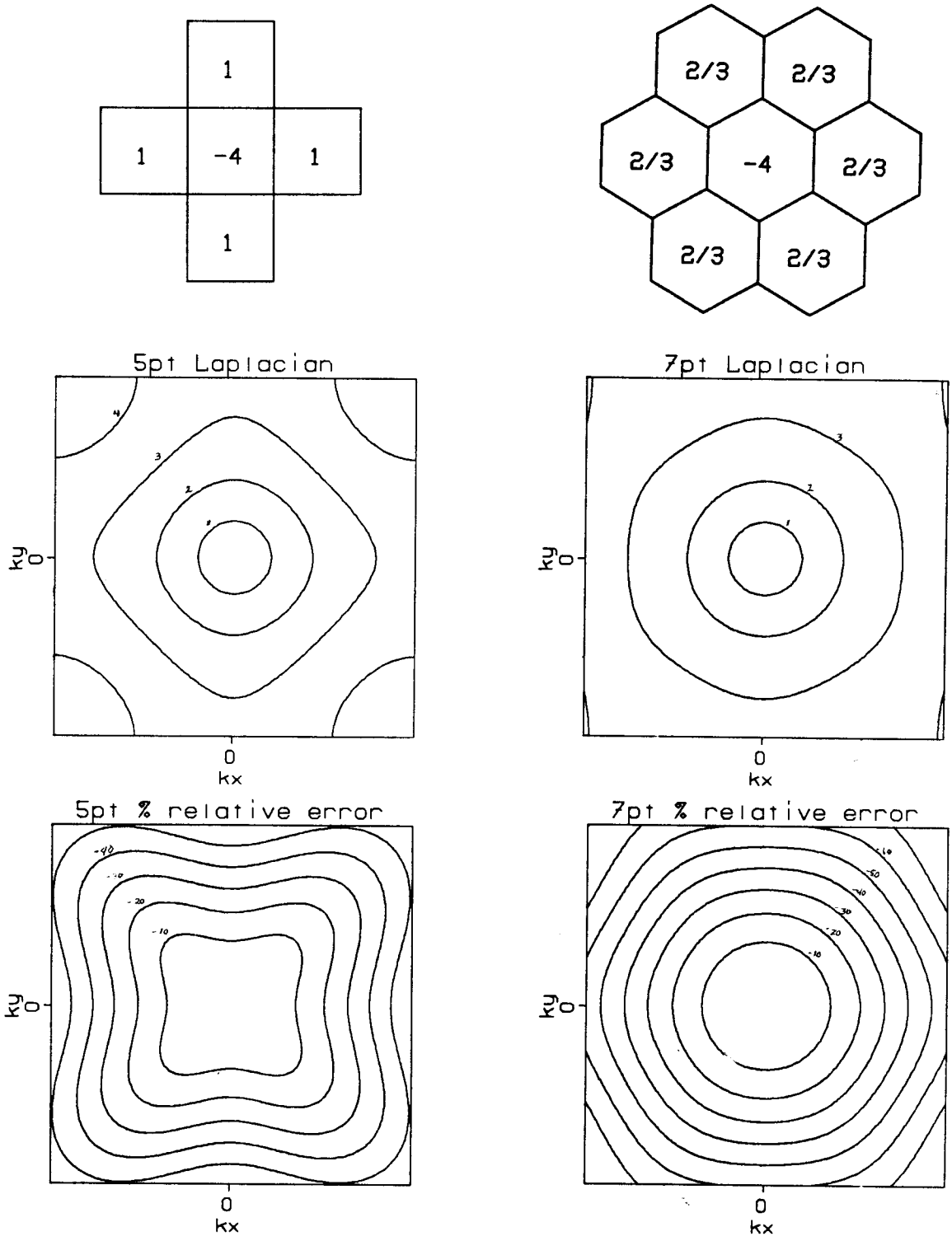

FIG. 4a. $O\left(\Delta x^2\right)$ leggy square and hexagonal difference star approximations of the Laplacian, their Fourier transforms, and the relative error between their transforms and the true Laplacian of Figure 3. Relative error is contoured at intervals of 10%, the Laplacian at intervals of (Nyquist)^2/5. k_x and k_y range from -Nyquist to Nyquist.

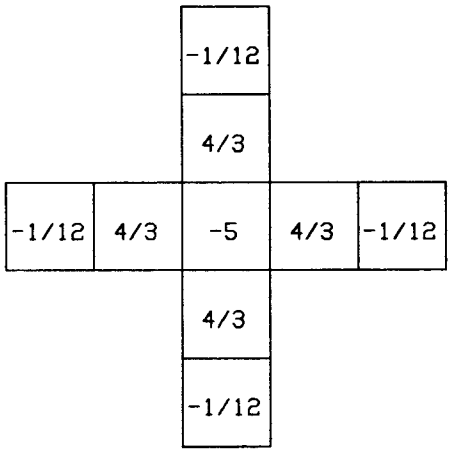

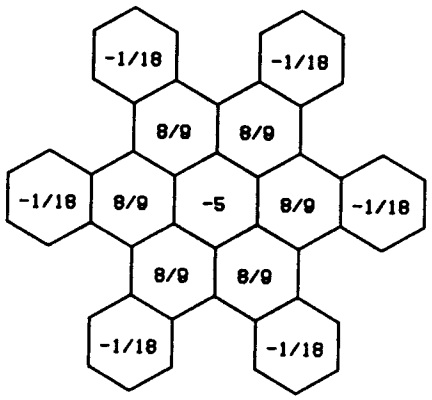

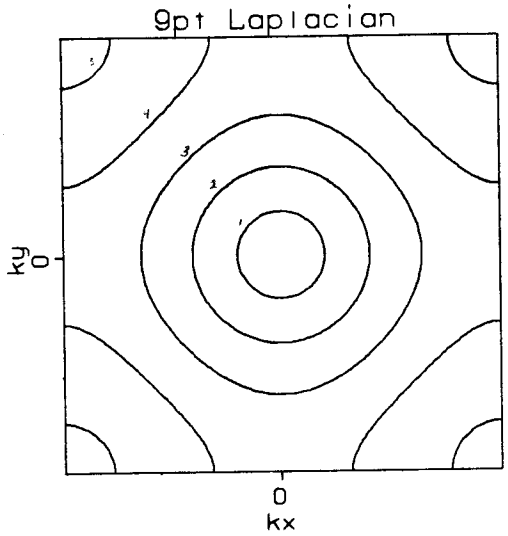

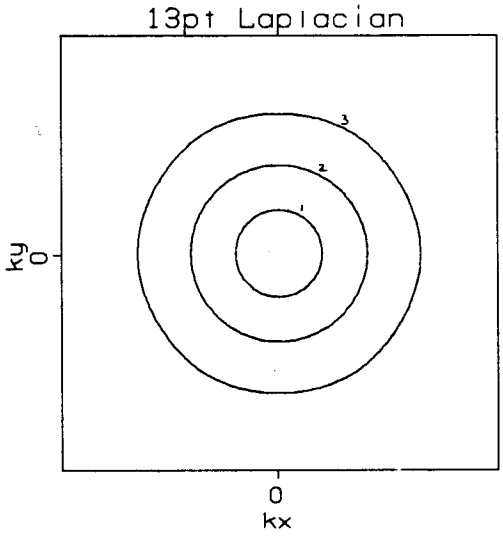

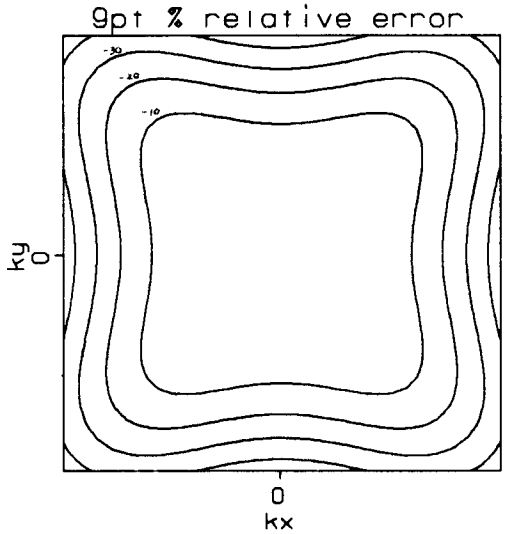

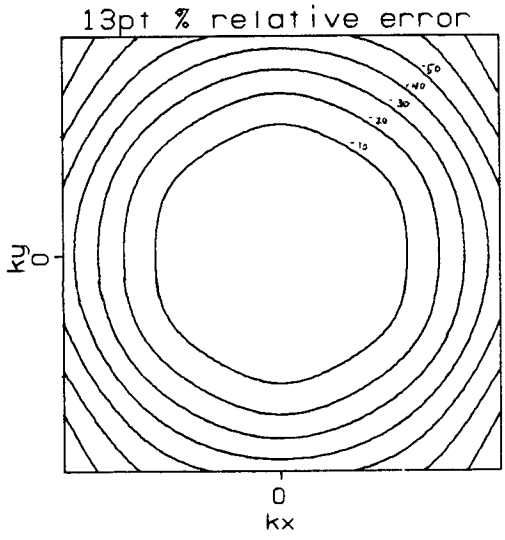

FIG. 4b. $O(\Delta x^4)$ leggy square and hexagonal difference star approximations of the Laplacian, their Fourier transforms, and the relative error between their transforms and the true Laplacian of Figure 3. Relative error is contoured at intervals of 10%, the Laplacian at intervals of (Nyquist)^2/5. k_x and k_y range from –Nyquist to Nyquist.

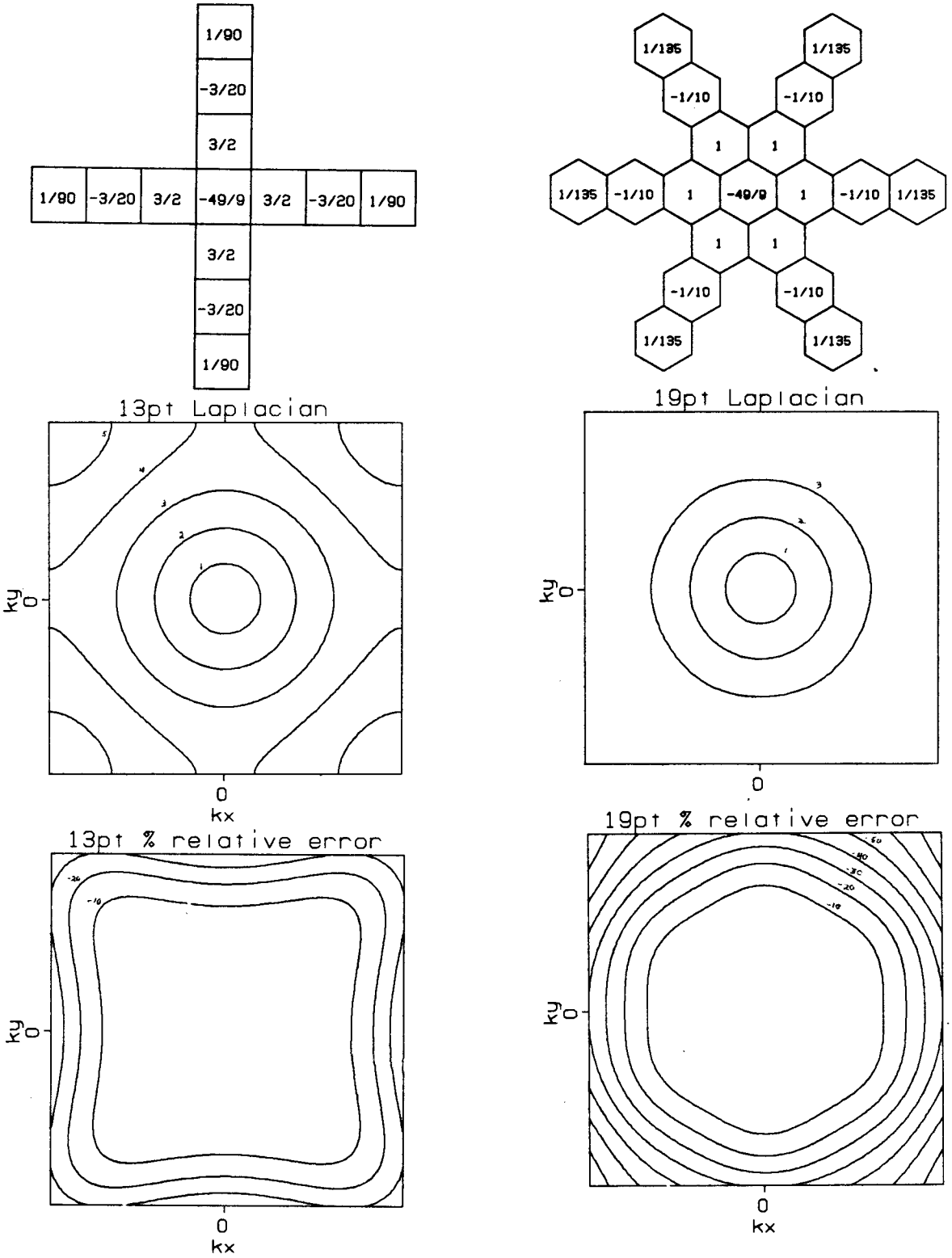

FIG. 4c. $O\left(\Delta x^6\right)$ leggy square and hexagonal difference star approximations of the Laplacian, their Fourier transforms, and the relative error between their transforms and the true Laplacian of Figure 3. Relative error is contoured at intervals of 10%, the Laplacian at intervals of (Nyquist)^2/5. k_x and k_y range from –Nyquist to Nyquist.

symmetry. While migration with any of the illustrated operators would be dispersive (the larger the operator the less the dispersion), the hexagonal operators would treat energy travelling in different directions most equally.

B. Compact operators

The preceding difference stars were designed through application of a one-dimensional design rule of linear extension and truncation. In two dimensions a second rule becomes possible—that of forming maximally compact, space-filling operators. In Figure 2 this alternate rule corresponds to differencing along the dotted as well as the solid line directions; in equation (5) it corresponds to summing over m sets of n truncated, symmetrically distributed, one-dimensional second derivatives. Because the method involves combining distinct approximations of the Laplacian accurate to distinct orders of distinct Δx_i's, the Taylor series accuracy of the composite operator can no longer be determined through inspection of equation (5). Instead, each sampled point (u_i) in a compact style operator must be expressed as a Taylor series expansion around the central point (u_0), and the resulting set of linear equations combined to remove as many higher order terms in Δx as possible.

To illustrate the method, the expansions of the 5 and 7 point operators of Figure 4a to the 9 and 13 point compact operators of Figure 5 are detailed below. First, the symmetry of the desired 9 and 13 point patterns permits Taylor series expansion of a full ring of points at a time: for the square, 9 point pattern $(\Delta x = \sqrt{3}h/2)$

$$\sum_{i=1}^{4} u_i = 4u_0 + \Delta x^2 \left(\frac{\partial^2 u}{\partial x^2} + \frac{\partial^2 u}{\partial y^2}\right)\Big|_{u_0} + \frac{\Delta x^4}{12}\left(\frac{\partial^4 u}{\partial x^4} + \frac{\partial^4 u}{\partial y^4}\right)\Big|_{u_0} + O(\Delta x^6) \tag{6}$$

$$\sum_{i=5}^{8} u_i = 4u_0 + 2\Delta x^2 \left(\frac{\partial^2 u}{\partial x^2} + \frac{\partial^2 u}{\partial y^2}\right)\Big|_{u_0} + \frac{\Delta x^4}{6}\left(\frac{\partial^4 u}{\partial x^4} + \frac{6\partial^4 u}{\partial x^2 \partial y^2} + \frac{\partial^4 u}{\partial y^4}\right)\Big|_{u_0} + O(\Delta x^6);$$

for the hexagonal 13 point pattern $(\Delta x = h)$

$$\sum_{i=1}^{6} u_i = 6u_0 + \frac{3}{2}\Delta x^2 \left(\frac{\partial^2 u}{\partial x^2} + \frac{\partial^2 u}{\partial y^2}\right)\Big|_{u_0} + \frac{3}{32}\Delta x^4 \left(\frac{\partial^2 u}{\partial x^2} + \frac{\partial^2 u}{\partial y^2}\right)^2\Big|_{u_0} + O(\Delta x^6) \tag{7}$$

$$\sum_{i=7}^{12} u_i = 6u_0 + \frac{9}{2}\Delta x^2 \left(\frac{\partial^2 u}{\partial x^2} + \frac{\partial^2 u}{\partial y^2}\right)\Big|_{u_0} + \frac{27}{32}\Delta x^4 \left(\frac{\partial^2 u}{\partial x^2} + \frac{\partial^2 u}{\partial y^2}\right)^2\Big|_{u_0} + O(\Delta x^6).$$

Second, recognizing $\left(\partial^2 u/\partial x^2 + \partial^2 u/\partial y^2\right)|_{u_0}$ as the Laplacian, the equations are combined to cancel out as many higher order terms as possible: for the 9 point operator no

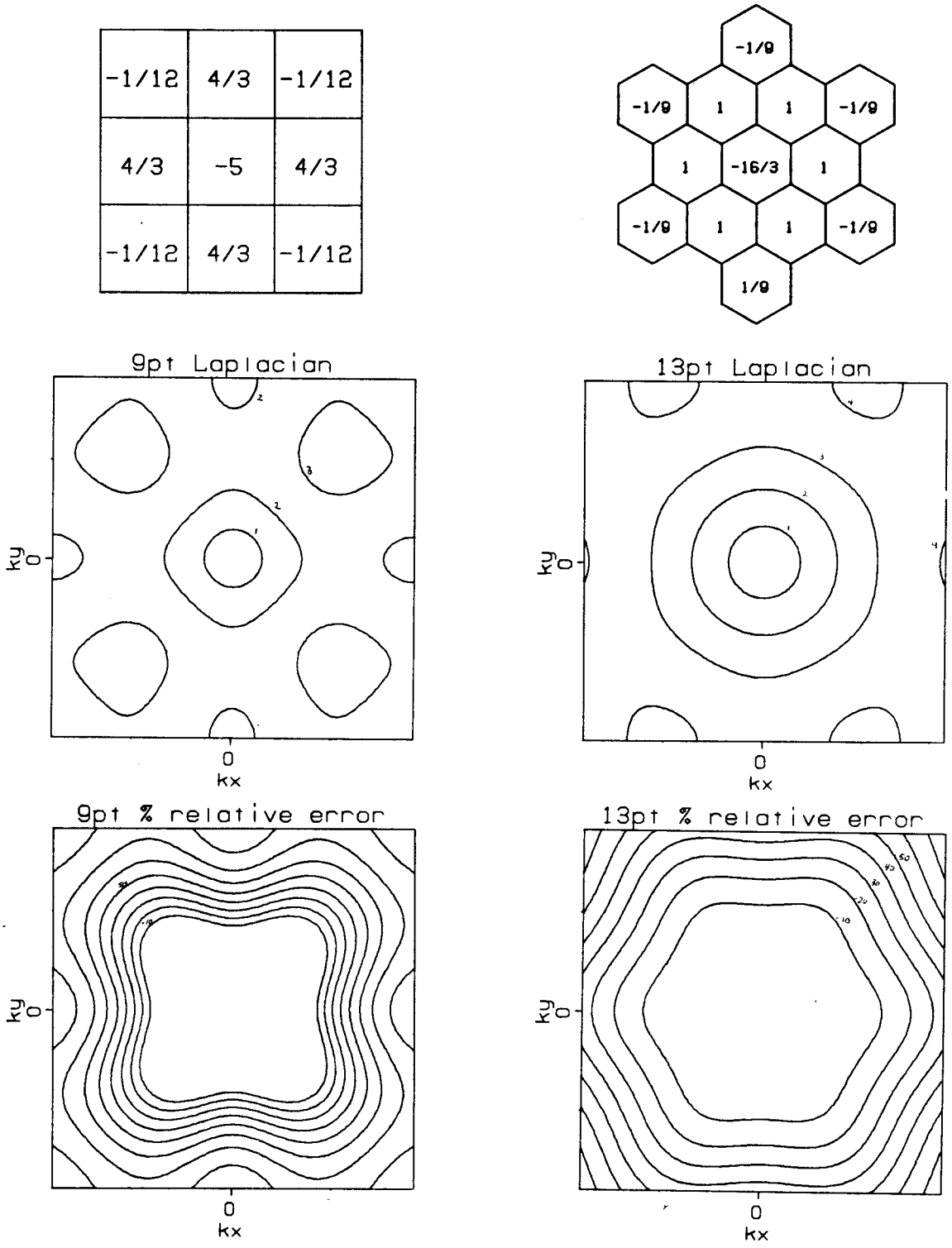

FIG. 5. Compact square $O(\Delta x^2)$ and hexagonal $O(\Delta x^2)$ difference star approximations of the Laplacian, their Fourier transforms, and the relative error between their transforms and the true Laplacian of Figure 3. Relative error is contoured at intervals of 10%, the Laplacian at intervals of (Nyquist)^2/5. k_x and k_y range from -Nyquist to Nyquist.

higher order terms can be eliminated

$$\frac{1}{\Delta x^2}\left(\frac{1}{3}\sum_{i=5}^{8} u_i + \frac{1}{3}\sum_{i=1}^{4} u_i - \frac{8}{3}u_0\right) = \nabla^2 + O(\Delta x^2); \tag{8}$$

for the 13 point operator, terms are cancelled through $O(\Delta x^4)$

$$\frac{1}{\Delta x^2}\left(-\frac{1}{3}\sum_{i=7}^{12} u_i + \frac{1}{3}\sum_{i=1}^{6} u_i - \frac{16}{3}u_0\right) = \nabla^2 + O(\Delta x^4). \tag{9}$$

The coefficients for the sample points become the weights in the difference stars.

The examples show these compact operators require many more points to achieve the same Taylor series accuracy as their leggy counterparts. The first compact, square mesh pattern accurate to $O\left(\Delta x^4\right)$ is the 8-direction, 17 point star of Figure 6 (Rosenbach, 1953); the first compact hexagonal star accurate to $O\left(\Delta x^6\right)$ requires more than 31 points. While the square 17 point operator demonstrates greater circular symmetry than its 9 point counterpart, the hexagonal 13 point compact operator is less circular than its leggy equal. Unless characterized by greater stability, the space-filling method appears far less efficient than the linear extension method in generating accurate difference formula approximations to the Laplacian.

Explicit schemes: 45 degree wave equation

Circular symmetry arguments aside, the accuracy of explicit 3-d migration may also be increased through use of a 45 degree wave equation. Among many other 45 degree formulæ, a strict Taylor series expansion of the paraxial wave equation yields

$$\frac{\partial P}{\partial z} \approx \frac{-i\omega}{v} - \frac{1}{2}\left(\frac{v}{-i\omega}\right)\nabla^2 - \frac{1}{4}\left(\frac{v}{-iw}\right)^3 \nabla^4. \tag{10}$$

Hidden within ∇^4 is the cross term $\partial^4/\partial x^2 \partial y^2$. While this term may be represented on any leggy, hexagonal mesh difference star, it can not be represented on any leggy, square mesh star (contemplate equations (6) and (7) and/or the Appendix). The necessity of abandoning the leggy pattern with a square operator suggests explicit, 45 degree wave equation migration may be implemented most efficiently on a hexagonal sampling mesh.

Implicit schemes

Given the desirability of solving tridiagonal systems, implicit 3-d migration schemes rely on splitting. For square meshes, a 2-way split, 1/6-trick, Crank-Nicolson formulation

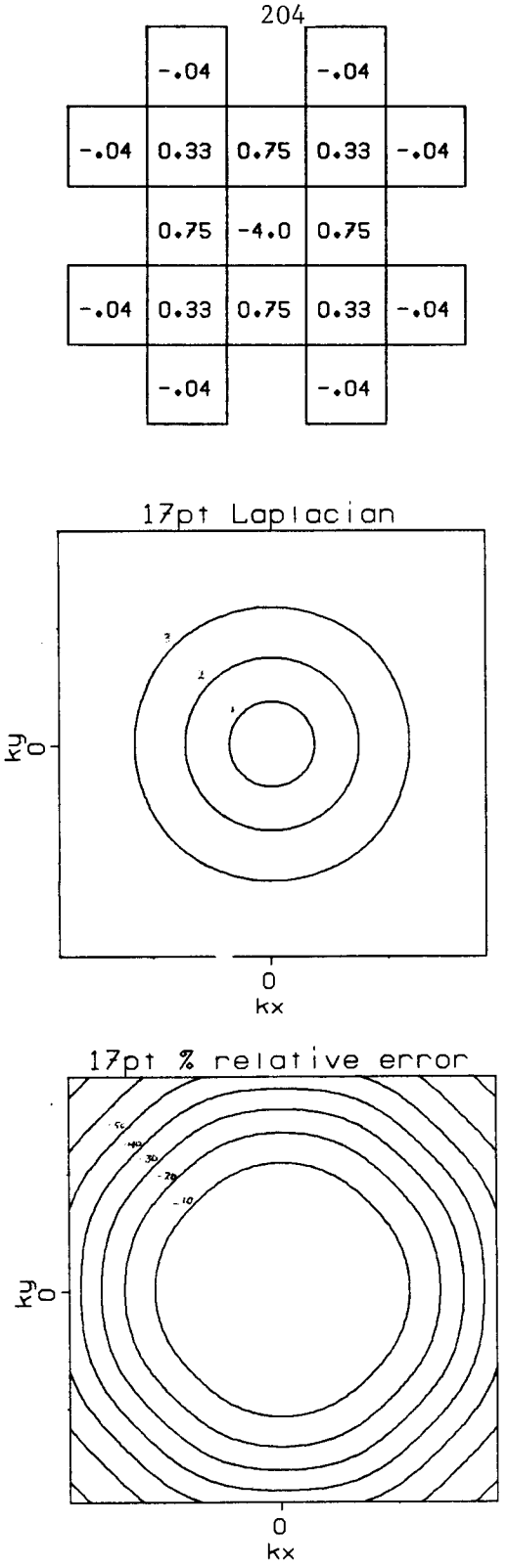

FIG. 6. $O\left(\Delta x^4\right)$ compact 17 point square difference star approximation of the Laplacian, its Fourier transform, and the relative error between its transform and the true Laplacian of Figure 3. Relative error is contoured at intervals of 10%, the Laplacian at intervals of (Nyquist)^2/5. k_x and k_y range from –Nyquist to Nyquist.

of the 15 degree retarded time wave equation diffraction term involves sequential solution of the relations

$$\frac{\partial Q}{\partial z} \approx -2\frac{v}{-2i\omega}\left(\frac{\frac{\delta^2}{\delta x^2}}{1+\frac{\Delta x^2}{n}\frac{\delta^2}{\delta x^2}}\right) \tag{11}$$

$$\frac{\partial Q}{\partial z} \approx -2\frac{v}{-2i\omega}\left(\frac{\frac{\delta^2}{\delta y^2}}{1+\frac{\Delta y^2}{n}\frac{\delta^2}{\delta y^2}}\right)$$

(Clærbout, 1984). Because the Laplacian may be represented as a summation of any n symmetrically distributed, one-dimensional second derivatives, these relations have identical 3-way split, hexagonal analogues

$$\frac{\partial Q}{\partial z} \approx -3\frac{v}{-2i\omega}\left(\frac{\frac{\delta^2}{\delta x_1^2}}{1+\frac{\Delta x_1^2}{n}\frac{\delta^2}{\delta x_1^2}}\right) \tag{12}$$

$$\frac{\partial Q}{\partial z} \approx -3\frac{v}{-2i\omega}\left(\frac{\frac{\delta^2}{\delta x_2^2}}{1+\frac{\Delta x_2^2}{n}\frac{\delta^2}{\delta x_2^2}}\right)$$

$$\frac{\partial Q}{\partial z} \approx -3\frac{v}{-2i\omega}\left(\frac{\frac{\delta^2}{\delta x_3^2}}{1+\frac{\Delta x_3^2}{n}\frac{\delta^3}{\delta x_2^2}}\right).$$

While the prospect of migrating and imaging in three directions as opposed to two may be disturbing, it must be remembered that hexagonal sampling requires 13.4% fewer samples than its square counterpart (see preceding paper). Furthermore, the redundancy of the nonorthogonal hexagonal axes may offer some yet to be determined advantages in dealing with lateral inhomogeneity.

Conclusion

The near circular symmetry of hexagonal sampling meshes results in hexagonal finite difference operators more successful than their square counterparts at approximating the two-dimensional Laplacian—and consequently at approximating the 3-d paraxial wave equation. Much work remains to be done to determine the extent of their advantages and disadvantages in explicit and implicit migration schemes.

Appendix

Equation (3) will be proven in the frequency domain, where it becomes

$$k^2 = \frac{2}{n}\sum_{\alpha=1}^{n} k_\alpha{}^2. \tag{13}$$

In words this relation implies that the squared distance of any point from the origin is equal to $2/n$ times the sum of the squares of its projections along any n symmetrically distributed (equally spaced) axes—a generalized form of the Pythagorean theorem. Considering a set of n symmetrically distributed directions (the first direction oriented at some angle ϕ with respect to the x axis) the right hand side of equation (12) becomes

$$\begin{aligned}
&\frac{2k^2}{n}\sum \cos^2\left(\phi+\frac{\alpha\pi}{n}\right)\\
&\quad=\frac{2k^2}{n}\left[\sum_{\alpha=0}^{n-1} cos^2\phi\cos^2\frac{\alpha\pi}{n}+\sum_{\alpha=0}^{n-1}\sin^2\phi\sin^2\frac{\alpha\pi}{n}-2\sin\phi\cos\phi\sum_{\alpha=0}^{n-1}\sin\frac{\alpha\pi}{n}\cos\frac{\alpha\pi}{n}\right]\\
&\quad=\frac{2k^2}{n}\left[\cos^2\phi\sum_{\alpha=0}^{n-1}\cos^2\frac{\alpha\pi}{n}+\sin^2\phi\sum_{\alpha=0}^{n-1}\sin^2\frac{\alpha\pi}{n}\right]\\
&\quad=\frac{2k^2}{n}\left[\cos^2\phi\sum_{\alpha=0}^{n-1}\left(\frac{1}{2}+\frac{1}{2}\cos 2\frac{\alpha\pi}{n}\right)+\sin^2\phi\sum_{\alpha=0}^{n-1}\left(\frac{1}{2}-\frac{1}{2}\cos 2\frac{\alpha\pi}{n}\right)\right]\\
&\quad=\frac{2k^2}{n}\left[\frac{n}{2}\cos^2\phi+\frac{n}{2}\sin^2\phi\right]\\
&\quad=k^2. \qquad (14)
\end{aligned}$$

Acknowledgements

We wish to thank Joe Dellinger for writing plotting programs making Figure 2 and the difference stars of Figures 4, 5 and 6 possible.

References

Clærbout, J.F., 1984, Imaging the earth's interior: in press (sections 2.4 and 4.3).

Mitchell, A.R., and Griffiths, D.F., 1980, The finite difference method in partial differential equations: John Wiley and Sons, Chichester (p. 20).

Rosenbach, O., 1953, A contribution to the computation of the second derivative from gravity data: Geophysics, v. 18, p. 894-912.